MECSOL 2022 - Proceedings of the 8th International Symposium on Solid Mechanics
M.L. Bittencourt, J. Labaki, L.C.M. Vieira Jr. and E. Mesquita (Editors), Campinas SP, Brazil, October 17th to 19th, 2022

Exploring programmable defect modes in electromechanically coupled metastructures

Danilo Beli[1], Renan Lima Thomes[1] and Carlos De Marqui Jr.[1]

[1]São Carlos School of Engineering, University of São Paulo, Brazil

In this work, we propose a piezoelectric metamaterial beam with a periodic array of local electromechanical resonators to localize and transfer bending vibration energy. The motivation is to open new possibilities for programmable wave localization and vibration manipulation using smart electromechanical metamaterials with applications that may involve guiding, sensing, monitoring and harvesting. Differently from traditional metamaterials with fixed functions, smart metamaterials can be programmed by updating the electrical properties without the drawback of affecting the mechanical design. This feature opens possibilities for a superior wave and vibration control in architected materials since the mechanical properties can be modulated in time. A finite element approach based on Euler-Bernoulli theory for a piezoelectric bimorph beam is used to model and to investigate the wave and dynamic behavior of the smart metamaterial. Due to coupling physics (i.e., electrical and mechanical domains), a modified formulation has been used to apply the Bloch-Floquet theory in a super-cell to investigate the band gap and the defect mode. The periodic configuration, where all resonant circuits are tuned to the same frequency, has a band gap, i.e., a frequency range where the flexural wave cannot propagate. When one of the resonant circuits has a resonant frequency significantly different, compared to the other cells, a spatial defect is created. Therefore, a defect mode appears inside the band gap. Since this mode is protected by the band gap of the neighboring unit cells, vibration energy localizes spatially around the defected unit cell. We show that the defect can be modulated in space-time by updating the electrical resonance of subsequent unit cells in a smooth and synchronized strategy. As a consequence, the vibration energy is transferred along the metamaterial beam, and hence, perfectly localized according to the final defect position.
Keywords: electromechanical metamaterials, wave localization, space-time modulation, programmable materials

INTRODUCTION

Phononic crystals (Sigalas and Economou, 1992) and dynamic metamaterials (e.g., elastic and acoustic) (Liu et al., 2000) are engineered structures with the ability to modify the wave propagation through band gaps, i.e. frequency bands where waves cannot propagate. The band gaps of phononic crystals open due to periodic mismatch of properties (e.g., geometry and material) at wavelengths comparable to the spatial periodicity and where incident and reflect waves cancel each other leading to the Bragg scattering (Sigalas and Economou, 1992). On the other hand, metamaterials open band gaps due to arrays of local resonating attachments, which provide interesting and unusual dynamic properties at low frequencies (Liu et al., 2000; Hussein et al., 2014). Due to their unique wave manipulation capabilities, phononic crystals and metamaterials have been used for a wide variety of applications over the past two decades, such as acoustic and vibration isolation (Sánchez-Pérez et al., 1998; Ho et al., 2003; Bilal and Hussein, 2013), cloaking (Cummer and Schurig, 2007; Norris and Shuvalov, 2011), focusing (Guenneau et al., 2007), sound collimation (Chen et al., 2004; Christensen et al., 2007) and refraction of sound waves (Cervera et al., 2001; Zhang and Liu, 2004; Hussein et al., 2014).

An important feature for various applications of engineered structures is the wave localization and guidance using defects (Sigalas, 1997, 1998; Torres et al., 1999; Kafesaki et al., 2001; Khelif et al., 2003a). In metamaterials, a point defect is created by replacing a local resonator with another one that has significantly different dynamic properties (Kaina et al., 2017). By introducing a point defect, the local periodicity is broken and a flat pass band (or defect band) emerges within the band gap (Sigalas, 1997; Shakeri et al., 2019). Therefore, energy can be confined inside and at the vicinity of the defect, resulting in wave localization. In addition, line defects are created when a chain of unit cells is replaced by defects, resulting in a waveguide where elastic wave propagation is confined by the band gaps of the adjacent unit cells (Sigalas, 1998). If one cannot control the dynamic properties of resonant attachments of metamaterials, the elastic wave manipulation through defects in such periodic systems would be limited to fixed configurations (Liu et al., 2000; Martínez-Sala et al., 1995; Beli et al., 2019; Wang et al., 2020). Therefore, efforts towards tunable architected materials have been reported in the literature (Wang et al., 2020), paving the way for remarkable applications such as tunable wave localization (Hu et al., 2014; Shakeri et al., 2019); reconfigurable wave guiding (Wang et al., 2017; Jin et al., 2016; Casadei

et al., 2012; Oh et al., 2011; Li et al., 2019) with filtering (Khelif et al., 2003b) and (de)multiplexing properties (Pennec et al., 2004; Mohammadi and Adibi, 2011; Rostami-Dogolsara et al., 2016; Vasseur et al., 2011; Wang et al., 2017); as well as new concepts on vibration-based energy harvesting (Carrara et al., 2013; Oudich and Li, 2017; Jo et al., 2020, 2021).

Tunable or programmable phononic crystals and metamaterials are usually obtained by mechanical or multifield coupling-based reconfigurability (Wang et al., 2020). Among different possibilities for multifield coupling, piezoelectric materials are a relatively popular choice (Thorp et al., 2001; Wu et al., 2009; Spadoni et al., 2009; Airoldi and Ruzzene, 2011; Casadei et al., 2012, 2010; Wang et al., 2014; Oh et al., 2011; Shakeri et al., 2019; Li et al., 2019; Yi et al., 2019; Sugino et al., 2020b,a; Silva et al., 2020). In such case, the wave behavior of electromechanically coupled metamaterials and phononic crystals can be controlled by updating external passive shunt circuits or active circuits (Wu et al., 2009; Wang et al., 2014; Shakeri et al., 2019; Thorp et al., 2001; Airoldi and Ruzzene, 2011; Spadoni et al., 2009; Casadei et al., 2010; Yi et al., 2019; Sugino et al., 2020b). Electromechanically coupled phononic crystals can realize arbitrarily (reconfigurable) shaped waveguides by short-circuiting selected paths of piezoelectric inclusions while leaving the remaining units in open-circuit condition (Oh et al., 2011). Bragg scattering band gap of a plate with periodic array of cylindrical stubs combined with piezoelectric resonators allows the control of elastic waves propagation through pre-configured waveguides of the phononic crystal (Casadei et al., 2012). Piezoelectric material connected to negative capacitance circuits can also tune the propagation direction in relatively complex shaped waveguides of elastic metamaterial plates (Li et al., 2019), realizing switchable waveguides. Recently, the use of digitally controlled analog circuits (Silva et al., 2020) and digital shunt circuits (Sugino et al., 2020a) replacing analog shunts has facilitated experimental implementations of reconfigurable and programmable matamaterials.

In this work, we present a programmable piezoelectric metamaterial that can confine elastic energy and perform space-time wave localization by programming defects in a periodic array of electromechanical resonators. The manipulation of localized waves in space and time is induced by strategically controlling the inductance of shunt circuits (i.e., local resonators) connected to the electromechanical unit cells of a beam.

ELECTROELASTIC MODEL

Consider an elastic beam composed of a conductive substructure bracketed by two piezoelectric layers oppositely poled in the z direction (i.e., a bimorph configuration) as in Fig. 1. The piezoelectric layers are covered on top and bottom surfaces by thin layers of conductive electrodes that are periodically segmented and connected in series to inductive shunt circuits, which are the local resonators. The boundaries of each segmented electrode region delimit the unit cell of the periodic electromechanical metamaterial depicted in Fig. 1. While the unit cells are electrically independent from each other, the right boundary of the j-th unit cell and the left boundary of the unit cell $j+1$ share the same mechanical degrees of freedom (DOFs).

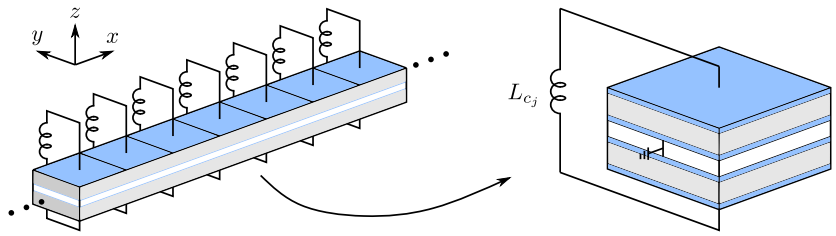

Figure 1 – Electromechanical metamaterial beam in a bimorph configuration (left) and its unit cell in detail (right). The colored regions correspond to the substructure (white), the piezoelectric material (gray), the electrodes (blue) and the shunt circuits composed by inductors L_c (black).

The Euler-Bernoulli assumptions are employed in the formulation of an electromechanically coupled finite element (FE) model of the metamaterial beam. The continuum is discretized into one-dimensional beam elements, each one containing two nodes at its boundaries. In the model derivation, the non-zero electric field component (z direction) is assumed uniform in the thickness direction of the piezoelectric element and the effect of structural damping is not taken into account. Therefore, the dynamic behavior of the electromechanical metamaterial beam can be described by the following finite element equations (Carpenter, 1997; De Marqui Junior et al., 2009):

$$\mathbf{M}\,\ddot{\mathbf{u}} + \mathbf{K}\,\mathbf{u} - \mathbf{P}\,\mathbf{v} = \mathbf{F} \tag{1}$$

$$\mathbf{C_p}\,\mathbf{v} + \mathbf{q} + \mathbf{P^t}\,\mathbf{u} = \mathbf{0}\,, \tag{2}$$

where $\mathbf{M}$ is the global mass matrix $(m \times m)$, $\mathbf{K}$ is the global stiffness matrix $(m \times m)$, $\mathbf{P}$ is the electromechanical coupling matrix $(m \times e)$, $\mathbf{C_p}$ is the diagonal capacitance matrix $(e \times e)$, $\mathbf{F}$ is the vector of external mechanical forces $(m \times 1)$, $\mathbf{v}$ is the vector of voltage output from each unit cell $(e \times 1)$, $\mathbf{q}$ is the vector of electrical charges $(e \times 1)$, and $\mathbf{u}$ is the vector of mechanical DOFs $(m \times 1)$, which contains the transverse displacements and the rotations (about the y direction) associated to each node. Here, m and e refer to the number of mechanical and electrical DOFs, respectively. The over-dots denote time differentiation and t denotes the matrix transpose when used as a superscript, otherwise, it stands for time. Equations (1) and (2) can be represented by a system of equations, as described in **?**, which characterizes a multiphysics problem in which the mechanical and electrical domains are coupled by the off-diagonal terms of the matrices, i.e., the electromechanical coupling matrix $\mathbf{P}$. For the j-th unit cell, the inductive shunt combined with the effective capacitance of the bimorph results in a capacitive-inductive circuit whose resonant frequency is (Hagood and von Flotow, 1991)

$$\omega_{n_j} = 1/\sqrt{C_{p_j} L_{c_j}}. \tag{3}$$

where C_{p_j} and L_{c_j} are the capacitance of the j-th unit cell and the inductance of the j-th shunt circuit, respectively. Conversely, an electrical resonance can be tuned to a selected frequency by setting its inductance to $L_{c_j} = 1/(C_{p_j}\,\omega_{n_j}^2)$.

The spectral properties of a periodic structure can be obtained by applying Bloch-Floquet conditions at the unit cell boundaries and solving the resulting eigenvalue problem. The unit cell, or the supercell (a set of unit cells), can be modeled using a FE model (Orris and Petyt, 1974), such as the one that results in Eqs. (1) and (2). However, matrix symmetry is highly recommended for solving such eigenvalue problems (Everstine, 1981). Therefore, these equations are modified by time integrating its second line as well as multiplying the first line by -1, and also by using an auxiliary variable with $\dot{\xi} = \mathbf{v}$, which results in the symmetric matrix form,

$$\tilde{\mathbf{M}}\,\ddot{\mathbf{p}} + \tilde{\mathbf{C}}\,\dot{\mathbf{p}} + \tilde{\mathbf{K}}\,\mathbf{p} = \tilde{\mathbf{F}} \tag{4}$$

whose terms are detailed in (**?**). By assuming harmonic motion, spectral solutions can be imposed: $\mathbf{p}(\mathbf{t}) = \bar{\mathbf{p}}(\omega)e^{i\omega\mathbf{t}}$ and $\tilde{\mathbf{F}}(t) = \bar{\mathbf{F}}(\omega)e^{i\omega t}$, where ω is the angular frequency and i is the unit imaginary number. Accordingly, Eq. 4 is transformed from time to frequency domain. Furthermore, by applying the Bloch periodic conditions represented by the linear transformation $\mathbf{T}$ (which is also described in **?**), Eq. 4 is transformed from space to wavenumber. These transformations lead to following eigenvalue problem $\omega(\kappa)$

$$(-\omega^2\hat{\mathbf{M}} + i\omega\hat{\mathbf{C}} + \hat{\mathbf{K}})\hat{\mathbf{p}} = \mathbf{0}, \tag{5}$$

with the reduced matrices $\hat{\mathbf{M}}(\kappa) = \bar{\mathbf{T}}^{\mathbf{t}}\tilde{\mathbf{M}}\mathbf{T}$, $\hat{\mathbf{C}}(\kappa) = \bar{\mathbf{T}}^{\mathbf{t}}\tilde{\mathbf{C}}\mathbf{T}$ and $\hat{\mathbf{K}}(\kappa) = \bar{\mathbf{T}}^{\mathbf{t}}\tilde{\mathbf{K}}\mathbf{T}$. Finally, the eigenvalue problem is solved by sweeping through all values of κ along the first irreducible Brillouin zone Hussein et al. (2014), i.e., $\kappa \in [0\ \pi/\Delta]$, thus finding the eigenvalues ω_j and eigenvectors (or wave mode shapes) $\hat{\mathbf{p}}_j$ as a function of κ_j. $\hat{\mathbf{p}}_j$ depicts the spatial distribution of the DOFs, whereas κ_j is the phase change per unit length (Mace et al., 2005; Beli et al., 2019).

RESULTS

In the simulations, each unit cell is composed of an aluminum substructure bracketed by a pair of PMN-PT piezoelectric elements, which are oppositely poled in the z direction and connected in series to a resonant shunt circuit. The material properties values are presented in Table 1. The length and the width of each unit cell is 12.7 mm, the thickness of each piezoelectric layer is 0.25 mm while the substructure is 0.167-millimeter thick. Throughout this text, the frequencies are normalized by the velocity of the longitudinal wave considering the average properties of the composite structure. Therefore, the normalized frequency is $\Omega = \omega\Delta/\left(2\pi\sqrt{Y_{avg}/\rho_{avg}}\right)$, where Y_{avg} is the average Young's modulus and ρ_{avg} is the average density. Each unit cell is discretized into eight finite elements, to properly capture the wave propagation phenomenon.

The band structure of the piezoelectric metamaterial beam without and with a point defect is computed considering a supercell composed of 21 unit cells (i.e., $n = 21$). In the supercell technique (Sigalas, 1997), the equation that represents one single unit cell, Eq. 5, can be used for the dispersion computation of the supercell by changing only the correspondent finite element matrices and the periodicity length Δ. Fig. 2(a) displays the band structure of the periodic metamaterial (without defect) with the resonant frequency of each local resonator tuned to $\Omega_t = 6.44 \times 10^{-3}$ ($\Omega_{n_j} = \Omega_t\ \forall\ j$), which is referenced throughout this work as the tuning frequency. Figure 2(b) shows the band structure for the piezoelectric metamaterial beam with a defect introduced at the 11^{th} unit cell (mid-length). The resonance of the 11^{th} electromechanical local resonator is tuned to $2\Omega_t$ (i.e., $\Omega_{n_{11}} = 2\Omega_t$) by updating its inductance and, therefore, creating the defect. Since the resonant shunt of the defected unit cell works like an open circuit (compared to the behavior of the other unit cells that are

Table 1 – Material properties for the aluminum substructure and the PMN-PT.

Property	Value
Young's modulus of the substructure, Y_s	69 GPa
Mass density of the substructure, ρ_s	2700 kg/m^3
Mass density of the piezoelectric material, ρ_p	8120 kg/m^3
Elastic compliance at constant electric field, s_{11}^E	45.9×10^{-12} Pa^{-1}
Piezoelectric strain coefficient, d_{31}	-646×10^{-12} V/m
Piezoelectric permittivity constant at constant stress, ε_{33}^T	4.208×10^{-8} F/m

tuned to Ω_t), a defect band (the red line in Fig. 2(b)) is created within the band gap at $\Omega = 6.01 \times 10^{-3}$, which is the defect-mode frequency. Since the defect band has nearly zero group velocity, vibration energy is localized and confined around this defected unit cell at the defect frequency. Figure 2(c-h) displays the wave modes related to transverse displacements (Fig. 2(c, e, g)) and voltage outputs (Fig. 2(d, f, h)) calculated at $\kappa\Delta/\pi = 1$ for the metamaterial with a point defect. At the band gap limits (e.g., Fig. 2(c, d)) and at the propagating bands (e.g., Fig. 2(g, h)), the vibration energy is evenly distributed along the supercell. On the other hand, the wave modes at the defect-band frequency (Fig. 2(e, f)) shows that vibration energy is localized inside and in the vicinity of the defect, as expected for localized defect mode, and voltage output is mostly in the vicinity of the defect.

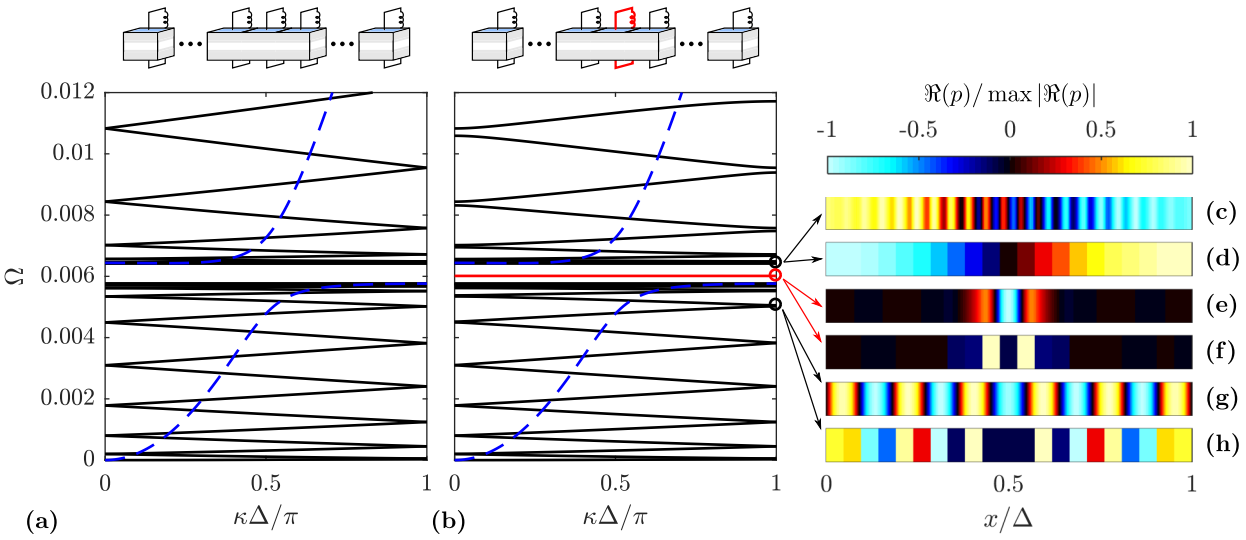

Figure 2 – Band structure of the periodic metamaterial (a) and metamaterial with defect (b): single unit cell $\Delta = a$ (blue dashed lines) and supercell with $\Delta = na$ (black and red lines). The displacement field (c, e, g) and the correspondent voltage field (d, f, g) for the wave mode shapes around the band gap (c-d and g-h) and at the defect band (e-f). The defect wave mode is depicted in red at the band structure (b).

Having characterized the behavior of the periodic and defected structures, now the space-time response of the piezoelectric metastructure with 21 unit cells is investigated. The Newmark method (Newmark, 1959) is employed to obtain the transient numerical solutions considering $\gamma = 1/2$ and $\beta = 1/4$, which is the same as assuming that $\ddot{\mathbf{u}} = (\ddot{\mathbf{u}}_{k+1} + \ddot{\mathbf{u}}_k)/2$, $\ddot{\mathbf{v}} = (\ddot{\mathbf{v}}_{k+1} + \ddot{\mathbf{v}}_k)/2$ and $\ddot{\mathbf{q}} = (\ddot{\mathbf{q}}_{k+1} + \ddot{\mathbf{q}}_k)/2$ within the interval (t_k, t_{k+1}) Petyt (1990). A constant time-step of 1.5783×10^{-5} s is considered in order to properly describe responses at frequencies up to of $\Omega = 0.008$. A point excitation is applied at the 11$^{\text{th}}$ unit cell (where the defect is originally placed) with a sine burst shape (sinusoidal envelope) and central frequency $\Omega = 6.01 \times 10^{-3}$ (the defect-mode frequency), magnitude 0.01 N and duration of 50 cycles.

The space-time wave localization is performed by the spatial-temporal modulation of a defect in the periodic array of electromechanical local resonators (i.e., the defect is programmable). While the unit cell with defect is gradually changed to the periodic array configuration by gradually tuning its electrical resonant frequency (i.e., electromechanical local resonator) to Ω_t, the shunt circuit of the subsequent unit cell is simultaneously updated from the periodic configuration Ω_t to open circuit (or to a significantly larger inductance such that $\Omega_{n_j} = 2\Omega_t$). Since vibration energy is localized in the

initial defect, we expect to transfer this energy between the adjacent unit cells and, finally, control the wave localization.

The rate of change of the local resonator frequency, $\mathrm{d}\Omega_n/\mathrm{d}t$, plays a significant role in the energy transfer over space and time. A perfect energy transition between subsequent unit cells is only accomplished by a smooth and synchronized changing of the local resonator frequencies, a key point for space-time wave localization by programmable defects. A fast transition (i.e., non-smooth) strategy, leads to vibration energy leak through the structure, avoiding the wave localization. A cosine function is employed to modulate the local resonator (i.e., shunt circuit) properties during the space-time transitions since its time derivative is zero at both beginning and end of the transition interval and $\mathrm{d}\Omega_n/\mathrm{d}t$ this function is continuous for every t. The transition speed and smoothness is controlled by its total duration $(t_f - t_0)$. For more details about the variation of the locally resonant frequency of the j-th unit cell, please check **?**.

Fig. 3(a) displays the transitions from unit cells 11, 12 and 13, which controls the space-time wave transport and localization. The envelope of the transverse displacement along the beam and of the voltage output from each unit cell are shown in Fig. 3(b, c), where the white dots delimits the stages I to V defined in Fig. 3(a). To further illustrate, Fig. 3(d-f) shows the displacement at the middle of unit cells 11, 12 and 13, while Fig. 3(g-i) shows the voltage outputs.

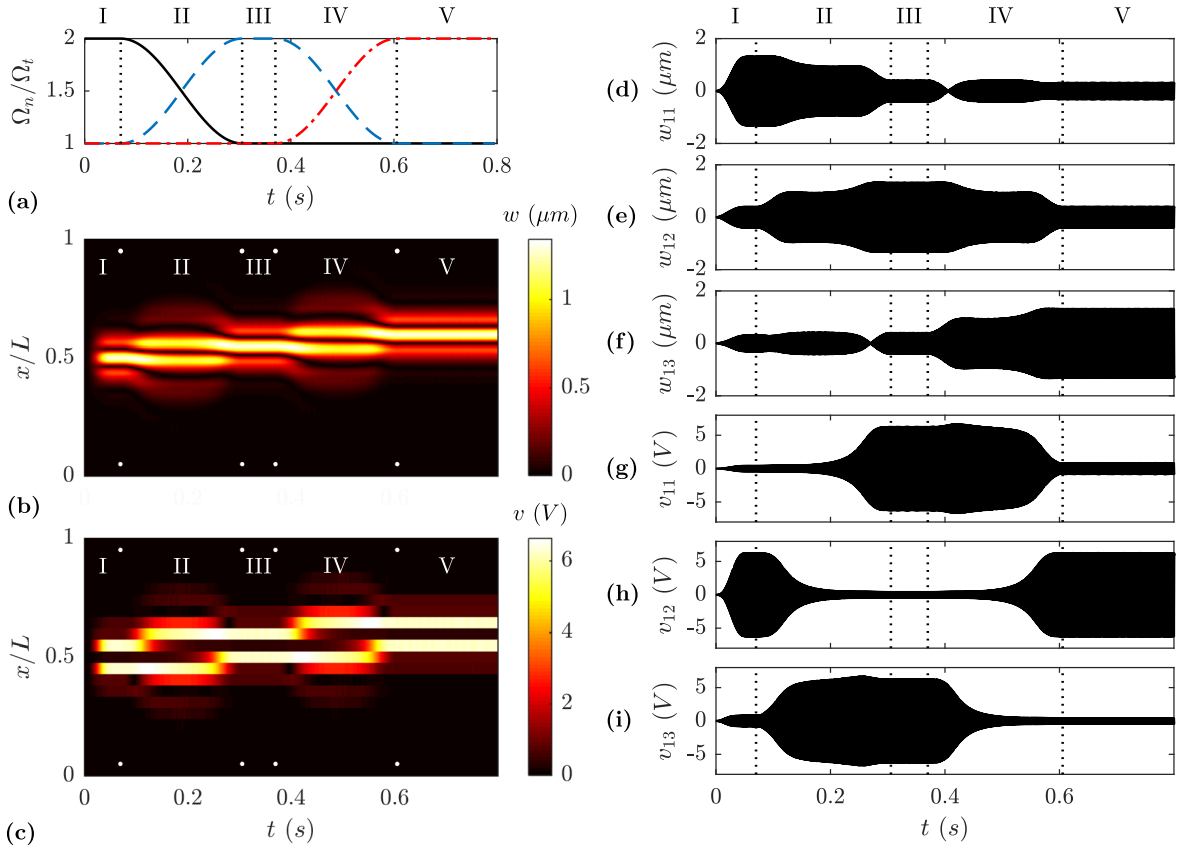

Figure 3 – Variation of the local resonator frequencies of unit cells 11 (continuous black), 12 (dashed blue) and 13 (dash-dotted red) (a). Envelope of the time response along the beam with a moving defect (b, c). Displacement at the middle of unit cells 11, 12 and 13 (x/L = 1/2, 23/42 and 25/42), respectively (d-f). Voltage output for cells 11, 12 and 13, respectively (g-i).

During stage I, unit cell 11 is a point defect since it is tuned to $2\Omega_t$ and all the other unit cells are tuned to Ω_t. Therefore, vibration energy is confined inside and in the vicinity of the unit cell 11, as can be observed in Fig. 3(b, d-f). At the beginning of stage II (from 0.07 s to 0.16 s), vibration amplitude at unit cell 11 is almost constant (Fig. 3(d)) since $\Omega_{n_{11}}/\Omega_t$ is slightly smaller than 2, while voltage output is low and constant (Fig. 3(g)). Simultaneously, the rate of change of mechanical amplitude at unit cell 12 is high (Fig. 3(e)) mostly due to energy flow from its own electrical attachment that is gradually detuned. From 0.16 s to 0.25 s, vibration amplitude at unit cells 11 and 12 is quite similar, as observed in Fig. 3(d, e). In the end of stage II, the amplitude of mechanical oscillations drops in unit cell 11 since it becomes tuned to Ω_t. Simultaneously, the amplitude of mechanical oscillations reaches a maximum in unit cell 12 since it becomes a defect. As depicted in Fig. 3(a), stage III characterizes a defect in unit cell 12 while all other unit cells are tuned to Ω_t. Figure 3(b, d-f) show that vibration energy has been transferred to unit cell 12, while low mechanical amplitude is observed in

unit cells 11 and 13, whose voltage output is high. Thus, space-time wave localization (from unit cell 11 to 12) due to programmable defects was performed during stages I to III. The behavior for stages III to V is quite similar to stages I to III and is omitted for brevity. In the end of the process of Fig. 3(a), the vibration energy is properly transferred and localized in unit cell 13, which is the final defect position.

CONCLUSIONS

A novel programmable piezoelectric metamaterial that can confine and transfer vibration energy along the structure by strategically programming point defects in space and time was presented. The point defect was introduced in the periodic array of electromechanical local resonators by properly tuning the electrical resonance of a unit cell (i.e. a local resonator). The vibration energy localized at a defected unit cell could be successfully transferred to a desired location of the metamaterial due to space-time modulated defects. The results in this work open new possibilities on wave localization (i.e., energy confinement) and manipulation (i.e., energy transferring) by using a smart electromechanical metastructures with programmable defects. Moreover, these concepts can be applied to wave devices with guiding, sensing, monitoring and harvesting capabilities.

ACKNOWLEDGMENTS

The authors gratefully acknowledge the support of the Brazilian National Council for Scientific and Technological Development (CNPq) through Grants 308690/2019-2, 433456/2018-3 and 130603/2019-8. The authors also acknowledge the support of the Sao Paulo Research Foundation (FAPESP) through project reference numbers 2018/18774-6 (postdoctorate fellowship) and 2018/15894-0 (research project "Periodic structure design and optimization for enhanced vibroacoustic performance: ENVIBRO").

REFERENCES

REFERENCES

Airoldi, L. and Ruzzene, M. (2011). Design of tunable acoustic metamaterials through periodic arrays of resonant shunted piezos. *New J. Phys.*, 13.

Beli, D., Fabro, A. T., Ruzzene, M., and Arruda, J. R. F. (2019). Wave attenuation and trapping in 3D printed cantilever-in-mass metamaterials with spatially correlated variability. *Sci. Rep.*, 9(1):1–11.

Bilal, O. R. and Hussein, M. I. (2013). Trampoline metamaterial: Local resonance enhancement by springboards. *Appl. Phys. Lett.*, 103(11):111901.

Carpenter, M. J. (1997). Using energy methods to derive beam finite elements incorporating piezoelectric materials. *J. Intell. Mater. Syst. Struct.*, 8(1):26–40.

Carrara, M., Cacan, M. R., Toussaint, J., Leamy, M. J., Ruzzene, M., and Erturk, A. (2013). Metamaterial-inspired structures and concepts for elastoacoustic wave energy harvesting. *Smart Mater. Struct.*, 22(6).

Casadei, F., Delpero, T., Bergamini, A., Ermanni, P., and Ruzzene, M. (2012). Piezoelectric resonator arrays for tunable acoustic waveguides and metamaterials. *J. Appl. Phys.*, 112(6).

Casadei, F., Ruzzene, M., Dozio, L., and Cunefare, K. A. (2010). Broadband vibration control through periodic arrays of resonant shunts: Experimental investigation on plates. *Smart Mater. Struct.*, 19(1).

Cervera, F., Sanchis, L., Sánchez-Pérez, J. V., Martínez-Sala, R., Rubio, C., Meseguer, F., López, C., Caballero, D., and Sánchez-Dehesa, J. (2001). Refractive Acoustic Devices for Airborne Sound. *Phys. Rev. Lett.*, 88(2):023902.

Chen, L.-S., Kuo, C.-H., and Ye, Z. (2004). Acoustic imaging and collimating by slabs of sonic crystalsmade from arrays of rigid cylinders in air. *Appl. Phys. Lett.*, 85(6):1072–1074.

Christensen, J., Fernandez-Dominguez, A. I., de Leon-Perez, F., Martin-Moreno, L., and Garcia-Vidal, F. J. (2007). Collimation of sound assisted by acoustic surface waves. *Nat. Phys.*, 3(12):851–852.

Cummer, S. A. and Schurig, D. (2007). One path to acoustic cloaking. *New J. Phys.*, 9(3):45–45.

De Marqui Junior, C., Erturk, A., and Inman, D. J. (2009). An electromechanical finite element model for piezoelectric energy harvester plates. *J. Sound Vib.*, 327(1-2):9–25.

Everstine, G. (1981). A symmetric potential formulation for fluid-structure interaction. *J. Sound Vib.*, 79(1):157–160.

Guenneau, S., Movchan, A., Pétursson, G., and Anantha Ramakrishna, S. (2007). Acoustic metamaterials for sound focusing and confinement. *New J. Phys.*, 9(11):399–399.

Hagood, N. and von Flotow, A. (1991). Damping of structural vibrations with piezoelectric materials and passive electrical networks. *J. Sound Vib.*, 146(2):243–268.

Ho, K. M., Cheng, C. K., Yang, Z., Zhang, X. X., and Sheng, P. (2003). Broadband locally resonant sonic shields. *Appl. Phys. Lett.*, 83(26):5566–5568.

Hu, A., Zhang, X., Wu, F., Yao, Y., Cheng, C., and Huang, P. (2014). Temperature effects on the defect states in two-dimensional phononic crystals. *Phys. Lett., Sect. A: Gen., Atomic Solid State Phys.*, 378(30-31):2239–2244.

Hussein, M. I., Leamy, M. J., and Ruzzene, M. (2014). Dynamics of phononic materials and structures: Historical origins, recent progress, and future outlook. *Appl. Mech. Rev.*, 66(4):1–38.

Jin, Y., Pennec, Y., Pan, Y., and Djafari-Rouhani, B. (2016). Phononic crystal plate with hollow pillars actively controlled by fluid filling. *Crystals*, 6(6).

Jo, S. H., Yoon, H., Shin, Y. C., Choi, W., Park, C. S., Kim, M., and Youn, B. D. (2020). Designing a phononic crystal with a defect for energy localization and harvesting: Supercell size and defect location. *Int. J. Mech. Sci.*, 179(April).

Jo, S.-H., Yoon, H., Shin, Y. C., and Youn, B. D. (2021). An analytical model of a phononic crystal with a piezoelectric defect for energy harvesting using an electroelastically coupled transfer matrix. *Int. J. Mech. Sci.*, 193(October 2020):106160.

Kafesaki, M., Sigalas, M. M., and García, N. (2001). Wave guides in two-dimensional elastic wave band-gap materials. *Phys. B: Condens. Matter*, 296(1-3):190–194.

Kaina, N., Causier, A., Bourlier, Y., Fink, M., Berthelot, T., and Lerosey, G. (2017). Slow waves in locally resonant metamaterials line defect waveguides. *Sci. Rep.*, 7(1):15105.

Khelif, A., Choujaa, A., Djafari-Rouhani, B., Wilm, M., Ballandras, S., and Laude, V. (2003a). Trapping and guiding of acoustic waves by defect modes in a full-band-gap ultrasonic crystal. *Phys. Rev. B - Condens. Matter Mater. Phys.*, 68(21):1–4.

Khelif, A., Deymier, P. A., Djafari-Rouhani, B., Vasseur, J. O., and Dobrzynski, L. (2003b). Two-dimensional phononic crystal with tunable narrow pass band: Application to a waveguide with selective frequency. *J. Appl. Phys.*, 94(3):1308–1311.

Li, G.-H., Wang, Y.-Z., and Wang, Y.-S. (2019). Active control on switchable waveguide of elastic wave metamaterials with the 3d printing technology. *Sci. Rep.*, 9(1):16226.

Liu, Z., Zhang, X., Mao, Y., Zhu, Y. Y., Yang, Z., Chan, C. T., and Sheng, P. (2000). Locally Resonant Sonic Materials. *Sci.*, 289(5485):1734–1736.

Mace, B. R., Duhamel, D., Brennan, M. J., and Hinke, L. (2005). Finite element prediction of wave motion in structural waveguides. *J. Acoust. Society Am.*, 117(5):2835–2843.

Martínez-Sala, R., Sancho, J., Sánchez, J. V., Gómez, V., Llinares, J., and Meseguer, F. (1995). Sound attenuation by sculpture. *Nat.*, 378(6554):241–241.

Mohammadi, S. and Adibi, A. (2011). On chip complex signal processing devices using coupled phononic crystal slab resonators and waveguides. *AIP Adv.*, 1(4):041903.

Newmark, N. M. (1959). A Method of Computation for Structural Dynamics. *J. Eng. Mech. Div.*, 85(3):67–94.

Norris, A. and Shuvalov, A. (2011). Elastic cloaking theory. *Wave Motion*, 48(6):525–538.

Oh, J. H., Kyu Lee, I., Sik Ma, P., and Young Kim, Y. (2011). Active wave-guiding of piezoelectric phononic crystals. *Appl. Phys. Lett.*, 99(8):2012–2015.

Orris, R. M. and Petyt, M. (1974). A finite element study of harmonic wave propagation in periodic structures. *J. Sound Vib.*, 33(2):223–236.

Oudich, M. and Li, Y. (2017). Tunable sub-wavelength acoustic energy harvesting with a metamaterial plate. *J. Phys. D: Appl. Phys.*, 50(31).

Pennec, Y., Djafari-Rouhani, B., Vasseur, J. O., Khelif, A., and Deymier, P. A. (2004). Tunable filtering and demultiplexing in phononic crystals with hollow cylinders. *Phys. Rev. E - Stat. Phys., Plasma, Fluids, Relat. Interdiscip. Top.*, 69(4):6.

Petyt, M. (1990). *Introduction to Finite Element Vibration Analysis*. Cambridge University Press, Cambridge.

Rostami-Dogolsara, B., Moravvej-Farshi, M. K., and Nazari, F. (2016). Designing Switchable Phononic Crystal-Based Acoustic Demultiplexer. *IEEE Trans. Ultrason., Ferroelectr. Freq. Control*, 63(9):1468–1473.

Sánchez-Pérez, J. V., Caballero, D., Mártinez-Sala, R., Rubio, C., Sánchez-Dehesa, J., Meseguer, F., Llinares, J., and Gálvez, F. (1998). Sound Attenuation by a Two-Dimensional Array of Rigid Cylinders. *Phys. Rev. Lett.*, 80(24):5325–5328.

Shakeri, A., Darbari, S., and Moravvej-Farshi, M. (2019). Designing a tunable acoustic resonator based on defect modes, stimulated by selectively biased PZT rods in a 2D phononic crystal. *Int. J. Solids Struct.*, 92:8–12.

Sigalas, M. and Economou, E. (1992). Elastic and acoustic wave band structure. *J. Sound Vib.*, 158(2):377–382.

Sigalas, M. M. (1997). Elastic wave band gaps and defect states in two-dimensional composites. *J. Acoust. Society Am.*,

101(3):1256–1261.

Sigalas, M. M. (1998). Defect states of acoustic waves in a two-dimensional lattice of solid cylinders. *J. Appl. Phys.*, 84(6):3026–3030.

Silva, T., Clementino, M., de Sousa, V., and De Marqui, C. (2020). An experimental study of a piezoelectric metastructure with adaptive resonant shunt circuits. *IEEE/ASME Trans. Mechatron.*, pages 1–1.

Spadoni, A., Ruzzene, M., and Cunefare, K. (2009). Vibration and wave propagation control of plates with periodic arrays of shunted piezoelectric patches. *J. Intell. Mater. Syst. Struct.*, 20(8):979–990.

Sugino, C., Ruzzene, M., and Erturk, A. (2020a). Digitally Programmable Resonant Elastic Metamaterials. *Phys. Rev. Appl.*, 13(6):1.

Sugino, C., Ruzzene, M., and Erturk, A. (2020b). Nonreciprocal piezoelectric metamaterial framework and circuit strategies. *Phys. Rev. B*, 102(1):1–7.

Thorp, O., Ruzzene, M., and Baz, A. (2001). Attenuation and localization of wave propagation in rods with periodic shunted piezoelectric patches. *Smart Mater. Struct.*, 10(5):979–989.

Torres, M., De Espinosa, F. R., García-Pablos, G. P., and García, N. (1999). Sonic band gaps in finite elastic media: Surface states and localization phenomena in linear and point defects. *Phys. Rev. Lett.*, 82(15):3054–3057.

Vasseur, J. O., Matar, O. B., Robillard, J. F., Hladky-Hennion, A. C., and Deymier, P. A. (2011). Band structures tunability of bulk 2D phononic crystals made of magneto-elastic materials. *AIP Adv.*, 1(4).

Wang, Y., Song, W., Sun, E., Zhang, R., and Cao, W. (2014). Tunable passband in one-dimensional phononic crystal containing a piezoelectric 0.62Pb(Mg1/3Nb2/3)O3-0. 38PbTiO3 single crystal defect layer. *Phys. E: Low-Dimens. Syst. Nanostructures*, 60:37–41.

Wang, Y.-F., Wang, T.-T., Wang, Y.-S., and Laude, V. (2017). Reconfigurable Phononic-Crystal Circuits Formed by Coupled Acoustoelastic Resonators. *Phys. Rev. Appl.*, 8(1):014006.

Wang, Y. F., Wang, Y. Z., Wu, B., Chen, W., and Wang, Y. S. (2020). Tunable and Active Phononic Crystals and Metamaterials. *Appl. Mech. Rev.*, 72(4).

Wu, L. Y., Wu, M. L., and Chen, L. W. (2009). The narrow pass band filter of tunable 1D phononic crystals with a dielectric elastomer layer. *Smart Mater. Struct.*, 18(1).

Yi, K., Ouisse, M., Sadoulet-Reboul, E., and Matten, G. (2019). Active metamaterials with broadband controllable stiffness for tunable band gaps and non-reciprocal wave propagation. *Smart Mater. Struct.*, 28(6).

Zhang, X. and Liu, Z. (2004). Negative refraction of acoustic waves in two-dimensional phononic crystals. *Appl. Phys. Lett.*, 85(2):341–343.

RESPONSIBILITY NOTICE

The authors are the only parties responsible for the printed material included in this paper.